High Temperature Material Processes 21(3):261–275 (2017)

MICROSTRUCTURE AND TRIBOLOGICAL PROPERTIES OF NITRIDE COATINGS BASED ON Zr, Ti, Cr, Nb, AND Si ELEMENTS

A.D. Pogrebnjak,[1] A.A. Bagdasaryan,[1] V.M. Beresnev,[2] A.I. Kupchishin,[3] S.V. Plotnikov,[4] & Ya.O. Kravchenko[1,]*

[1]*Sumy State University, 2 Rymsky Korsakov Str., Sumy, 40007, Ukraine*

[2]*Kharkiv National University, 21 Svoboda Sq., 4, Kharkiv, 61022, Ukraine*

[3]*Abai Kazakh National Pedagogical University, 13 Dostyk Ave., Almaty, 050010, Republic of Kazakhstan*

[4]*D. Serkbayev East Kazakhstan State Technical University, 69 A.K. Protozanov Str., Ust-Kamenogorsk, 070000, Republic of Kazakhstan*

*Address all correspondence to: Ya.O. Kravchenko, Sumy State University, 2 Rymsky Korsakov Str., Sumy, 40007, Ukraine, E-mail: mc.redline1991@gmail.com

The structure and tribological properties of the nitride coatings (Zr–Ti–Nb)N, (Zr–Ti–Cr–Nb)N, and (Zr–Ti-Cr–Nb–Si)N, fabricated by vacuum arc deposition have been investigated. Their elemental composition and crystal structure are characterized by EDS and SEM analyses, XPS, and X-ray diffraction. The multicomponent (Zr–Ti–Cr–Nb–Si)N and (Zr–Ti–Nb)N coatings are found to be a simple face-centered cubic (fcc) solid solution. For the coatings without Si, the structure is mainly composed of the TiN fcc phase and Cr_2N trigonal modification. The (Zr–Ti–Nb)N and (Zr–Ti–Cr–Nb)N coatings provided the best adhesive strength in different conditions. The (Zr–Ti–Cr–Nb–Si)N coatings exhibited the worst adhesive strength, which may be attributed to the relative low hardness

KEY WORDS: *vacuum arc, tribological properties, multielement coatings, microstructure, adhesion*

1. INTRODUCTION

The lifetime of tools for machining, cutting, drilling, and other working processes is significantly enhanced by the use of nitride or carbide protective coatings, owing to their high hardness, plasticity, good wear, thermal stability, and corrosion resistance (Holleck, 1986; Sundgren and Hentzell, 1986; Pogrebnyak et al., 2009, 2014a; Poplavsky et al., 2017; Svito et al.,

2017). Based on the design concept for traditional alloys and physical metallurgy, it is found that almost all nitride coatings are based on one principal metallic element, for example, TiN, ZrN, and CrN. However, owing to the requirement of higher working properties, multicomponent nitride coatings such as Ti–Al–N, Ti–Nb–N, Ti–Cr–N, Zr–Ti–N, Cr–Zr–N, Zr–Ti–Si–N, Zr–Nb–Ti–Cr–N, Ti–Al–Cr–N, Ti–Hf–Zr–V–Nb–N, and others are attracting more and more attention (Pogrebnjak et al., 2014b; Pal Dey and Deevi, 2003; Kim et al., 2008; Han et al., 2003; Boxman et al., 2000; Zhang et al., 2013). Many research groups reported that the additions of elements with different atomic sizes to binary and ternary nitride films would have a favorable effect on the mechanical and tribological properties of protective coatings.

The purpose of this work is to investigate the influence of the deposition parameters on the elemental and phase composition, mechanical and tribological properties of (Zr–Ti–Nb)N, (Zr–Ti–Cr–Nb)N, and (Zr–Ti–Cr–Nb–Si)N coatings.

2. EXPERIMENTAL

The cathodes made from Zr–Ti–Nb (Zr — 35 at.%, Nb — 35 at.%, Ti — 30 at.%), Zr–Ti–Cr–Nb (Cr — 37.39 at.%, Zr — 27.99 at.%, Nb — 22.30 at.%, Ti — 12.32 at.%), Zr–Ti–Cr–Nb (Cr — 37.39 at.%, Zr — 27.99 at.%, Nb — 22.30 at.%, Ti — 12.32 at.%), and Zr–Ti–Cr–Nb–Si (Cr — 17.08 at.%, Zr — 30.19 at.%, Nb — 9.67 at.%, Ti — 39.96 at.%, Si — 3.1 at.%) were prepared by electron-beam melting. Nitride coatings were obtained by vacuum arc deposition in a molecular nitrogen atmosphere on polished substrates (material — A 570 Grade 36 steel and silicon) using a Bulat-6 vacuum-arc device. The substrates were heated to 450°C before deposition. The distance between the substrates and the cathode was 250 mm. The parameters of deposition of the coatings are presented in Table 1.

The chemical compositions and morphology of the coatings were examined using a PEGASUS X-ray energy-dispersive spectrometer system, scanning electron microscopy/energy-dis-

TABLE 1: The deposition parameters of the (Zr–Ti–Nb)N, (Zr–Ti–Cr–Nb)N, and (Zr–Ti–Cr–Nb–Si)N coatings

No.	Deposited Material	I_a, A	P_N, Pa	U, V
1	Zr–Ti–Nb	95	0.05	– 100
2		95	0.5	– 100
1	Zr–Ti–Cr–Nb	110	0.3	– 100
2			0.7	– 100
3			0.3	– 200
4			0.7	– 200
1	Zr–Ti–Cr–Nb–Si	110	0.3	– 100
2		110	0.3	– 200

persive X-ray spectroscopy (SEM/EDX) JEOL JSM-6610 LV, and JEOL 7001TTLS with a voltage of 15–20 kV.

The chemical bonding state of the films was analyzed by X-ray photoelectron spectroscopy (XPS, EC 2401, USSR) using MgK_α radiation (E = 1253.6 eV). Prior to XPS measurements, the samples were sputter-etched in an argon plasma for 5 min.

The structure and phase composition were analyzed by X-ray diffraction (XRD) using D8 ADVANCE and DRON-4 diffractometers, under CuK_α irradiation. XRD patterns were taken in the point-by-point scanning mode with a step of 2θ = 0.02–0.2° in the range of angles 25–90°.

The nanohardness and elasticity modulus of the (Zr–Ti–Cr–Nb–Si)N coatings were measured using nanoindentation (Hysitron TI 950 TriboIndenter) with a Berkovich diamond indenter and a maximal load of 10,000 μN. We evaluated the hardness and elasticity modulus from load–no-load curves using the Oliver–Pharr method.

A REVETEST (CSM Instruments) scratch tester equipped with a 200-mm-tip radius Rockwell C diamond indenter was used to measure the adhesion of the (Zr–Ti–Nb)N, (Zr–Ti–Cr–Nb)N, and (Zr–Ti–Cr–Nb–Si)N coatings. To obtain reliable results, two scratches on the surface of a coating were made. The substrates for the deposition of coatings were steel 18Cr10NiTi cylinders with a diameter of 30.0 mm and a height of 5.0 mm.

The critical load responsible for the moment of the appearance of the first chevron cracks at the bottom of the scratches was defined as L_{C1}; L_{C2}, the time of the occurrence of chevron cracks at the bottom of the scratches; L_{C3}, the destruction has a cohesive-adhesive character; L_{C4}, the local flaking of the areas of coating, and L_{C5}, the plastic abrasion of a coating to the substrate, loss of adhesion strength.

First-principles band-structure calculations were carried out using the Quantum-ESPRESSO code (Giannozzi et al., 2009) for 8-atom cubic supercells of $Ti_{4-n}Nb_nN_4$, $Ti_{4-n}Zr_nN_4$, and $Zr_{4-n}Nb_nN_4$, n = 0, 1, 2, 3, 4, representing $Ti_{1-x}Nb_xN$, $Ti_{1-x}Zr_xN$, and $Zr_{1-x}Nb_xN$ alloys, respectively, with the B1 structure (space group Fm–3m, No. 225). The Vanderbilt ultra-soft pseudo-potentials were used to describe the electron–ion interaction (Vanderbilt, 1990).

To estimate the formation energies of the nitrides under consideration, the total energies of the Ti, Zr, Nb, Cr, and Si crystal as well as the N_2 molecule were calculated. The structures based on Cr were considered in the paramagnetic state. The structural parameters and formation energies of different calculated phases are listed in Table 2. The maximum deviations between theoretical and experimental values are observed for the structures based on Cr (since

TABLE 2: Symmetry, calculated structural parameters (a, c/a), and formation energies (E^f) of TiN, ZrN, NbN, CrN, Cr_2N, and Si_3N_4 in comparison with the available experimental data (in parentheses)

Structure	Symmetry	a, Å	c/a	E^f, eV/f.u.
TiN	Fm–3m No. 225	4.232 (4.241)[a]	—	– 3.490 (– 3.500)[b]
ZrN	Fm–3m No. 225	4.591 (4.600)[c]	—	– 3.512 (– 3.786)[b]

TABLE 2: *Continued*

Structure	Symmetry	*a*, Å	*c*/*a*	E^f, eV/f.u.
NbN	Fm–3m No. 225	4.420 (4.442)[d]	—	– 1.938 (– 2.432)[b]
CrN	Fm–3m No. 225	4.006 (4.140)[e]	—	– 0.511 (– 1.215)[b]
Cr_2N	P–31m No. 162	4.705 (4.811)[f]	0.924 (0.932)[f]	– 1.219 (– 1.337)
Si_3N_4	$P6_3$/m No. 176	5.659 (7.637)[g]	0.382 (0.383)[g]	– 7.580 (– 7.690)[b]
Ti	$P6_3$/mmc No. 194	2.919 (2.944)[h]	1.584 (1.589)[h]	—
Zr	$P6_3$/mmc No. 194	3.232 (2.232)[i]	1.601 (1.593)[i]	—
Nb	Im–3m No. 229	3.312 (3.311)[j]	—	—
Cr	Im–3m No. 229	2.796 (2.884)[k]	—	—
Si	Fd–3m No. 227	5.467 (5.430)[l]	—	—

we considered only paramagnetic states) and the B1-NbN structure (due to the substoichiometry of niobium nitrides).

3. RESULTS

The concentrations of all elements in the coatings are summarized in Table 3. The compositions of all nitride films are close to their original targets.

The chemical binding state and elemental composition of the (Zr–Ti–Cr–Nb)N coating were investigated by XPS (see Fig. 1) with peaks which associated with Ti 2p, Cr 2p, Zr 3d, Nb 3d, N 1s. Also the oxygen (O 1s) peak was observed. According to the existing data (Wagner, 1995), the Ti 2p peaks at 455.8 and 458.7 eV correspond to the Ti–O and Ti–N bonds, respectively; the Cr 2p peak at 576.1 eV corresponds to the Cr–N bond; the Zr 3d peaks at 180.1 eV and 182.2 eV, to the Zr–N and Zr–O bonds, respectively; the Nb 3d at 203.8 eV and 207.5 eV, to the Nb–N and Nb–O bonds, respectively; the N 1s peak at 397.4 eV, to the Cr–N bond, and the O 1s peak at 531.3 eV corresponds to the Nb–O bond. These results suggest that the (Zr–Ti–Cr–Nb)N coating consists of the Ti–N, Ti–O, Cr–N, Zr-N, Zr–O, Nb—N, and NB–O bonds which could be attributed to TiN, TiO_2, Cr_2N, ZrN, ZrO_2, NbN, and Nb_2O_5, respectively. Thus, it can be assumed that the coatings formed a multiphase material, (Ti, Zr, Nb)N–Cr.

TABLE 3: Elemental analysis of the (Zr–Ti–Nb)N, (Zr–Ti–Cr–Nb)N, and (Zr–Ti–Cr–Nb–Si)N coatings

Series No.	Concentration, at.%						
	Ti	Zr	Cr	Nb	N	Si	Impurity
	(Zr–Ti–Nb)N						
1	20.91	20.38	—	19.99	38.72	—	—
2	20.52	19.36	—	19.26	40.86	—	—
	(Zr–Ti–Cr–Nb)N						
1	10.21	6.63	15.22	4.96	62.41	—	0.57
2	12.30	8.48	16.92	6.17	56.13	—	—
3	11.27	8.03	18.23	7.48	54.99	—	—
4	10.40	7.81	11.00	6.73	63.66	—	0.39
	(Zr–Ti–Cr–Nb–Si)N						
1	34.50	11.58	11.00	3.30	36.49	2.12	—
2	32.30	13.28	7.95	3.62	39.5	3.45	—

Figure 2 shows the XRD patterns of (Zr–Ti–Nb)N nitride coatings. The X-ray diffractometer spectrum analysis shows that the determining phase composition is the phase with a face-centered cubic lattice. The low-intensity peak at $2\theta = 38°$ indicates the presence of small inclusions in the BCC lattice, typical of the vacuum-arc method for a dropping phase. A characteristic feature of increasing pressure of the reaction gas (from 0.05 Pa to 0.5 Pa) strengthens the peaks of the family of planes {111}, which is determined by the increase in the perfection of preferred orientation of growth of crystallites with the [111] axis perpendicular to the plane of the surface. Specific method of approximating the size of the crystallites with increase in pressure increases from 10 nm at the lowest pressure of 0.05 Pa to 63 nm at the maximum working pressure of nitrogen atmosphere of 0.5 Pa.

The phase analysis of (Zr–Ti–Cr–Nb)N nitride coatings indicates the presence of the TiN fcc phase (a = 0.243 nm, a_{tab} = 0.244 nm) and Cr_2N trigonal modification (P31m space group, a = 0.4800 nm, c = 0.4472 nm) (see Fig. 3). The formation of a two-phase structure is obviously related to the presence of high concentrations of Cr and Nb elements, which have a low enthalpy of formation of nitrides.

The results of XRD diffraction analysis for (Zr–Ti–Cr–Nb–Si)N coatings are shown in Fig. 4. As we can see, for a nitride coating deposited at a pressure of 0.3 Pa and substrate bias of – 100 V all XRD lines belonging to 111, 200, 220, 311, and 222 reflections from the fcc lattice are seen. Taking into account the elemental composition, we can state that this fcc phase belongs to the NaCl structure type, where the Zr, Cr, Ti, Si, and Nb atoms are located in the lattice sites.

The maximal value of hardness (44.5 GPa) for the (Zr–Ti–Nb)N nitride coating is reached at the pressure of reaction gas P_N = 0.5 Pa. The hardness of the (Zr–Ti–Cr–Nb)N coatings deposited at P_N = 0.3 Pa and U = – 100 V are 30.9 GPa which change to 38.8 GPa as the substrate inclination increases to – 200 V.

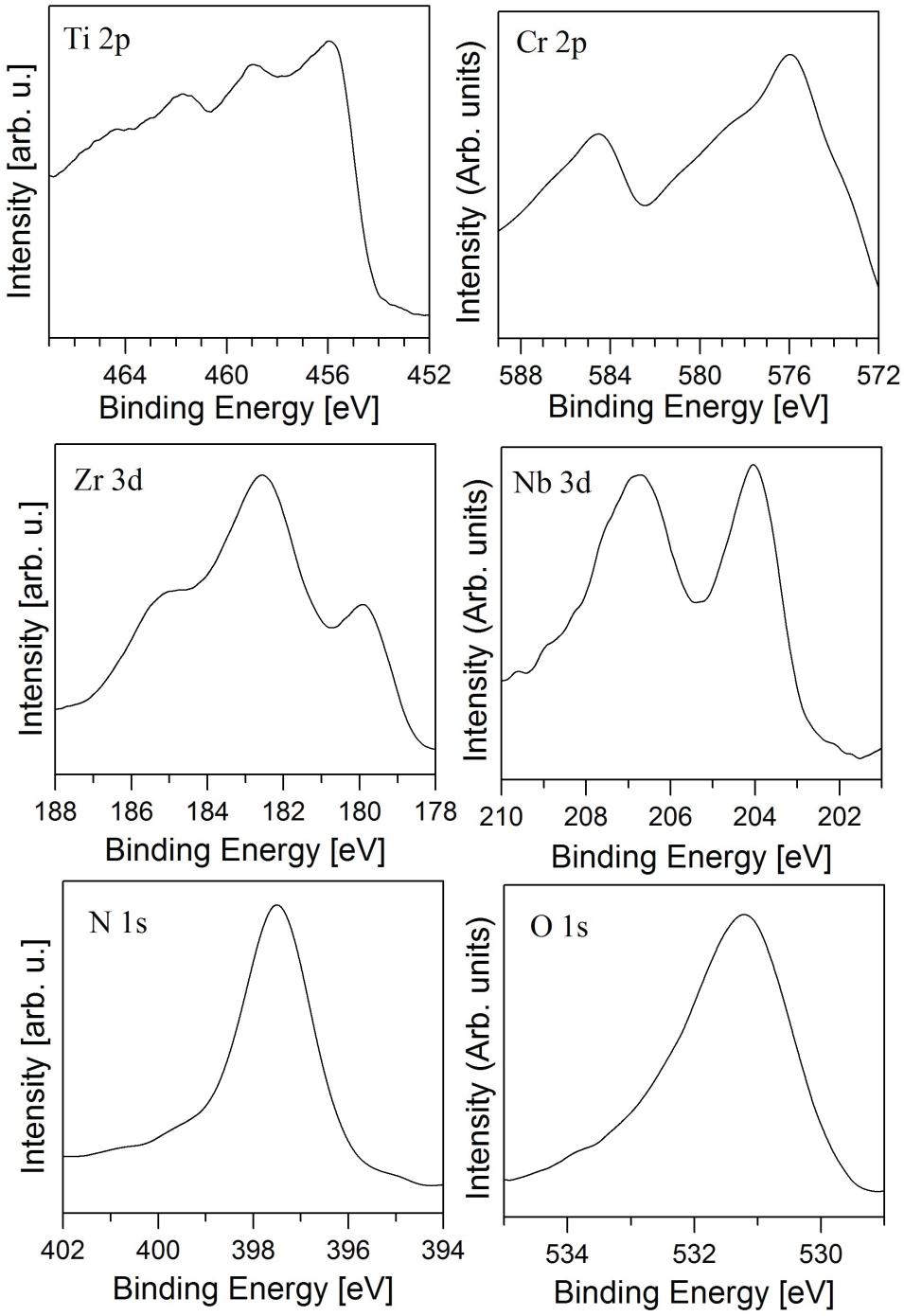

FIG. 1: XPS peaks of (Zr–Ti–Cr–Nb)N coating deposited at P_N = 0.3 Pa and U = 200 V

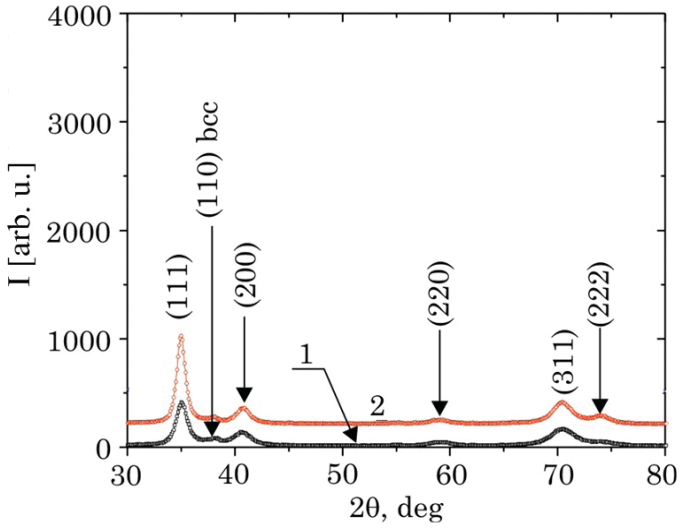

FIG. 2: Areas of diffraction spectra of (Zr–Ti–Nb)N coatings obtained at different partial pressures of nitrogen: 1) P_N = 0.05 Pa; 2) P_N = 0.5 Pa

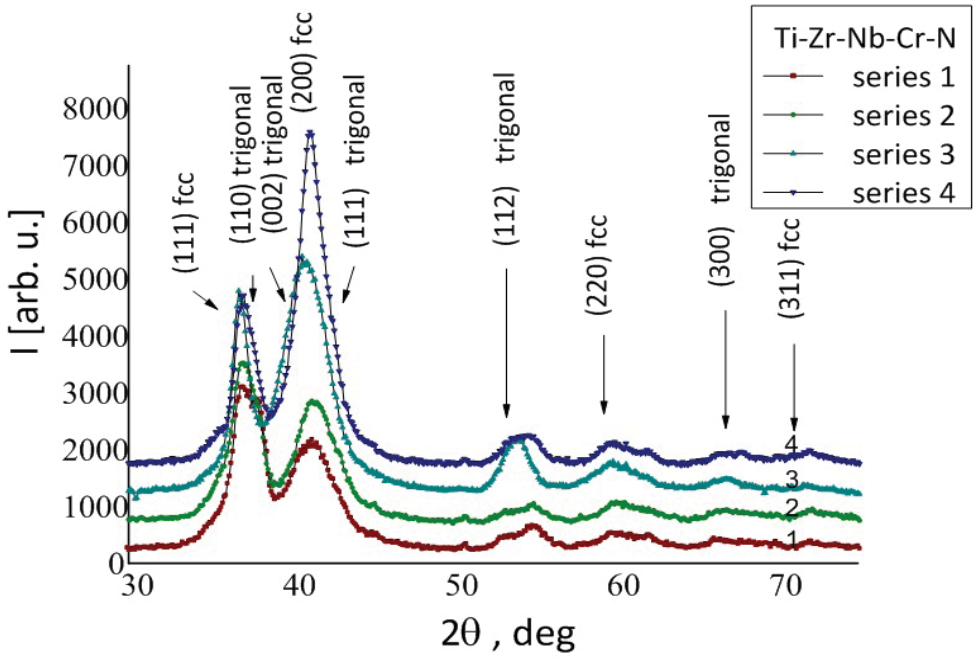

FIG. 3: XRD patterns of the (Zr–Ti–Cr–Nb)N nitride films deposited at different P_N and U values

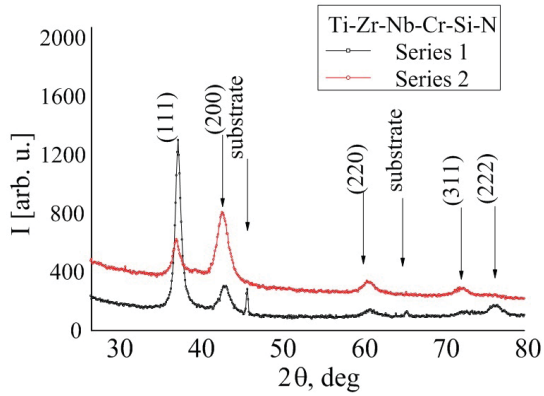

FIG. 4: XRD patterns of the (Zr–Ti–Cr–Nb–Si)N nitride films deposited at P_N = 0.3 Pa and different U values (– 100, – 200 V)

From the load–no-load curves of nanoindentation tests of (Zr–Ti–Cr–Nb–Si)N coatings, the nanohardness and modulus of the films deposited at different substrate inclinations were determined and shown in Fig. 5. For the (Zr–Ti–Cr–Nb–Si)N nitride coatings, which are deposited

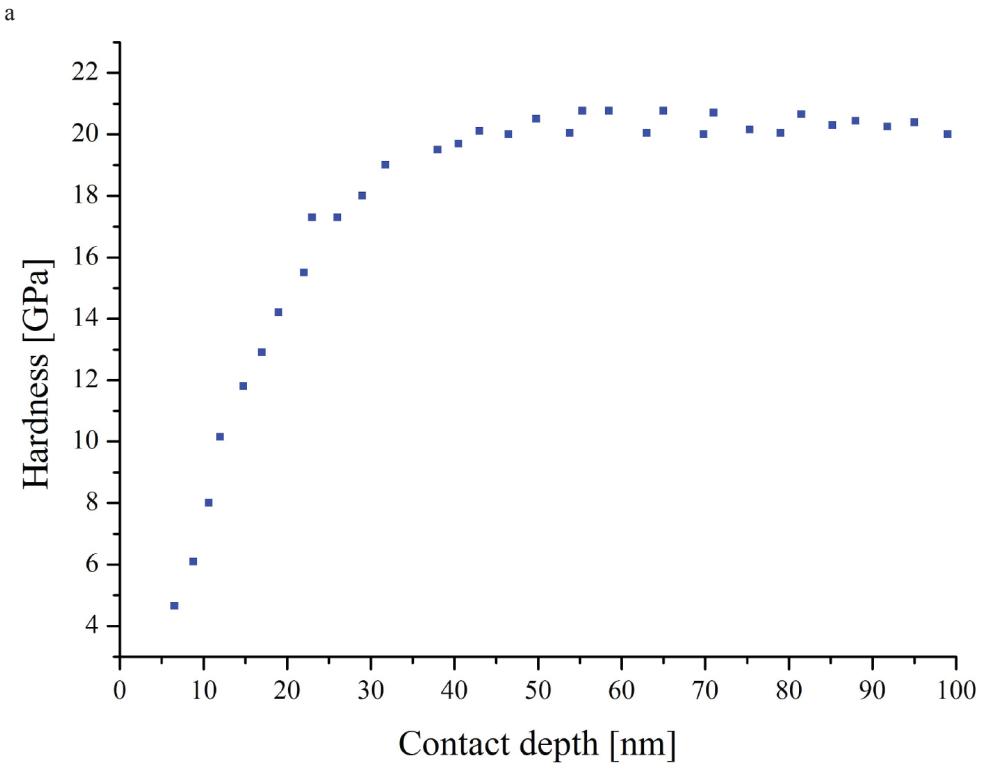

FIG. 5.

b

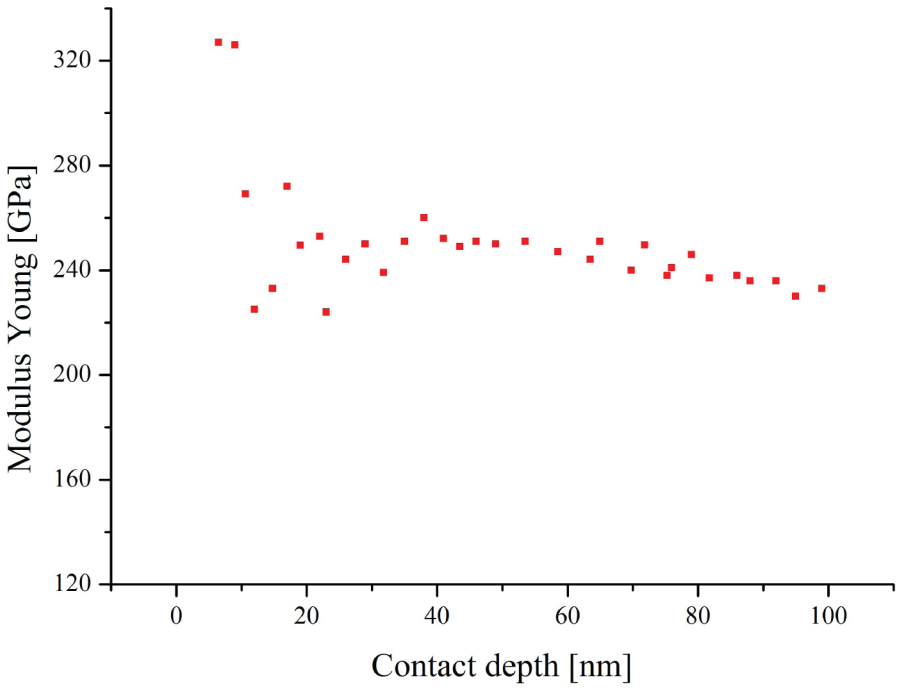
Modulus Young [GPa]
320
280
240
200
160
120
0
20
40
60
80
100
Contact depth [nm]

c

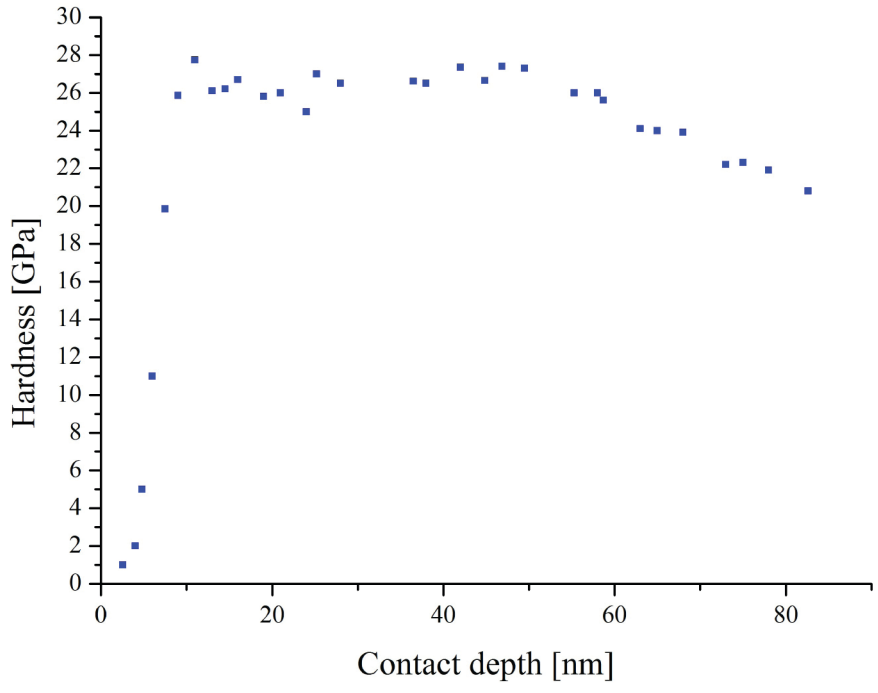
Hardness [GPa]
30
28
26
24
22
20
18
16
14
12
10
8
6
4
2
0
0
20
40
60
80
Contact depth [nm]

FIG. 5.

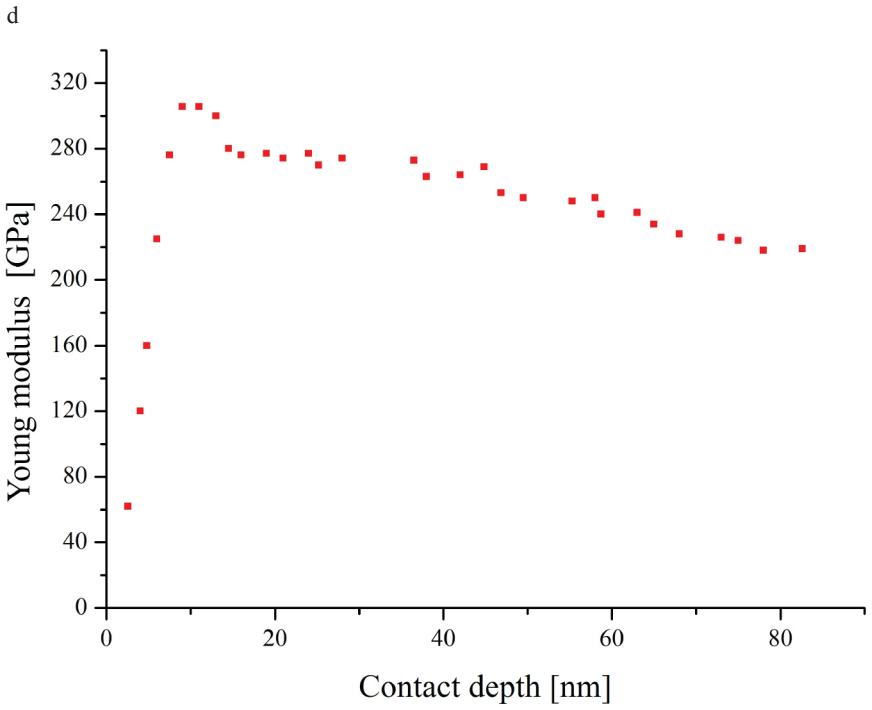

FIG. 5: Dependences of the hardness (a, c) and elastic modulus (b, d) on contact depth for (Zr–Ti–Cr–Nb–Si)N coatings deposited at P_N = 0.3 Pa and different U values: a, b) – 100 V, c, d) – 200 V

at P_N = 0.3 Pa and U = – 100 V, the hardness and elastic modulus are 21 and 250 GPa, respectively. With increase in the potential bias to – 200 V, the hardness and modulus increased to 27 and 273 GPa, respectively.

Table 4 shows the results of adhesion tests of the (Zr–Ti–Nb)N, (Zr–Ti–Cr–Nb–Si)N, and (Zr–Ti–Cr–Nb)N coatings obtained at different technological deposition parameters. The results of the adhesion strength tests show that the coatings were worn during scratching, but did not peel off, i.e., the destruction occurs by the cohesive mechanism, associated with the plastic deformation and formation of fatigue cracks in the coating material.

As shown in Table 4, with increasing substrate inclination, the adhesion strength between the coating and substrate increases. The enhanced adhesion may be attributed to the

TABLE 4: Comparative results of adhesion testing for the (Zr–Ti–Nb)N, (Zr–Ti–Cr–Nb)N, and (Zr–Ti–Cr–Nb–Si)N coatings

Critical Loads, N	Serial Number			
	No. 1	No. 2	No. 3	No. 4
	(Zr–Ti–Nb)N			
L_{C1}	2.91	9.89	—	—

TABLE 4: *Continued*

Critical Loads, N	Serial Number			
	No. 1	**No. 2**	**No. 3**	**No. 4**
L_{C2}	29.04	20.62	—	—
L_{C3}	43.18	36.43	—	—
L_{C4} (L_{C5})	59.26	66.77	—	—
	(Zr–Ti–Cr–Nb)N			
L_{C1}	10.94	11.8	10.35	15.21
L_{C2}	18.69	20.93	18.42	24.29
L_{C3}	26.95	30.35	23.12	33.45
L_{C4}	39.15	45.94	45.12	40.97
L_{C5}	49.09	56.17	61.08	62.06
	(Zr–Ti–Cr–Nb–Si)N			
L_{C1}	9.54	11.28	—	—
L_{C2}	12.48	14.04	—	—
L_{C3}	18.36	24	—	—
L_{C4}	29.86	34.09	—	—
L_{C5}	45.33	45.57	—	—

enhanced resistance of crack formation and plastic deformation. The loads (L_{C5}) for the (Zr–Ti–Cr–Nb)N and (Zr–Ti–Cr–Nb–Si)N coatings increase with the substrate inclination (from – 100 to – 200 V), their maxima are of 62.06 and 45.57 N, respectively. Also, it should be noted, that coatings obtained at a high bias and possessing higher hardness are more resistant. Nitride coatings (Zr–Ti–Nb), (Zr–Ti–Cr–Nb)N, and (Zr–Ti–Cr–Nb–Si)N with a good adhesion strength demonstrate high values of hardness, 45, 42, and 29 GPa, respectively.

4. DISCUSSION

According to the XRD patterns (see Fig. 1) of the (Zr–Ti–Nb)N nitride coatings, the fcc is the determining phase with the (111) out-of-plane preffered orientation.

The Gibbs free energy of mixing of the (Zr–Ti–Nb)N alloys under investigation, calculated at $T = 0$ K (i.e., formation energy, see Table 2), is presented in Fig. 6 as a function of the composition x. The positive formation energy implies that the $Ti_{1-x}Zr_xN$ alloys are not stable, and will decompose into TiN and ZrN with the chemical driving force E_{mix}. However, all alloys can be stabilized in some range of composition, depending on temperature, since the configurational entropy is always positive and promotes a decrease in the Gibbs free energy. Since the values of E_{mix} for $Ti_{1-x}Nb_xN$ and $Zr_{1-x}Nb_xN$ are very small and some of them are negative, these alloys can be stabilized as solid solutions at moderate temperatures. These findings confirm the possibility of the formation of fcc solid solutions based on TiN, ZrN, and NbN in thin films. Since in our films we observed only solid solutions based on these nitrides, one can sup-

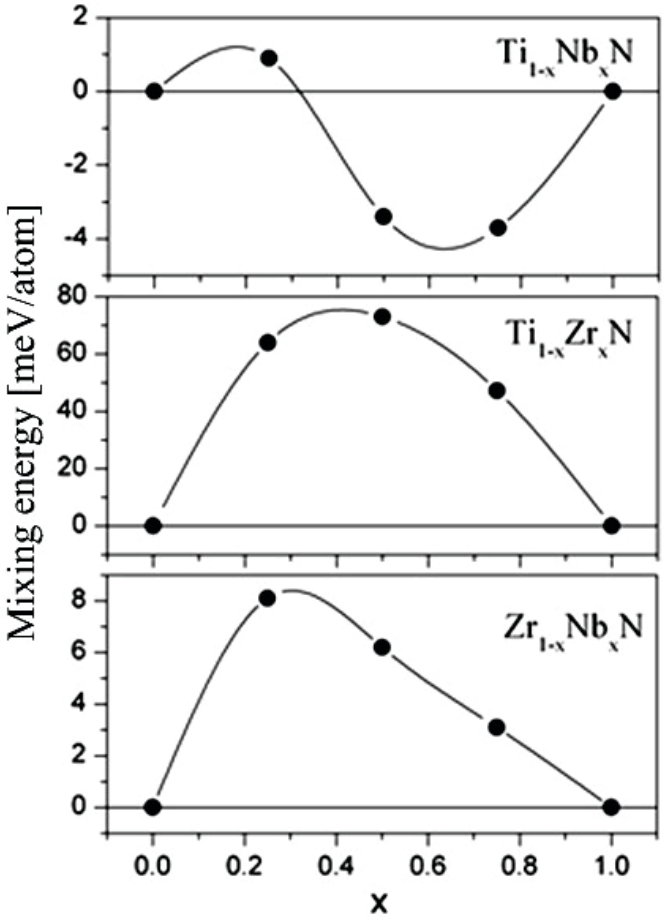

FIG. 6: Computed mixing energy E_{mix} of $Ti_{1-x}Nb_xN$, $Ti_{1-x}Zr_xN$, and $Zr_{1-x}Nb_xN$ alloys as a function of composition x

pose that the presence of NbN in the films precludes the separation of TiN and ZrN from the $Ti_{1-x}Zr_xN$ alloys. These findings confirm the possibility of the formation of fcc solid solutions based on TiN, ZrN, and NbN in thin films (Pogrebnjak et al., 2009, 2012, 2014b; Hasegawa et al., 2000; Sobol et al., 2011; Bagdasaryan et al., 2014). Since in our films we observed only solid solutions based on these nitrides, one can suppose that the presence of NbN in the films precludes the separation of TiN and ZrN from the $Ti_{1-x}Zr_xN$ alloys.

The analysis of diffraction data allowed us to estimate the lattice constant: a = 0.4365 nm for (Zr–Ti–Cr–Nb)N and a = 0.4332 nm for (Zr–Ti–Cr–Nb–Si)N coatings (see Table 5). This table reveals that the lattice constant of multicomponent coatings increases with the potential bias. This is reasonable because the intense bombardment causes incorporation of atoms of nitrogen into the spaces in the growing film that are smaller than the usual atomic volume ("atomic peening effect"). The grain sizes were calculated from the full width at half maximum of the XRD peaks by using the Scherrer formula. One obtains a typical grain size of 5.2 nm

TABLE 5: Lattice constants and grain sizes of the (Zr–Ti–Cr–Nb–Si)N and (Zr–Ti–Cr–Nb)N nitride films estimated by the XRD analysis

No.	Nitride Coating	Lattice Constant, nm	Grain Size, nm
1	(Zr–Ti–Cr–Nb)N	0.4365	5.2
2		0.4359	4.5
3		0.4410	5.1
4		0.4381	6.9
1	(Zr–Ti–Cr–Nb–Si)N	0.4332	11.5
2		0.4337	9.7

for the (Zr–Ti–Cr–Nb)N coating without preferential orientation and average crystallite size of 11.5 nm in the direction of growth of crystallites with [111] axis for (Zr–Ti–Cr–Nb–Si)N coatings.

As discussed previously, the coatings exhibit high hardness: 44.5 GPa for the (Zr–Ti–Nb)N nitride coating, 31–39 GPa for the (Zr–Ti–Cr–Nb)N coatings, and 21–27 GPa for the (Zr–Ti–Cr–Nb–Si)N coatings.

Several factors can explain the increasing hardness, namely, the residual stresses and film densification. The damages caused by the strong ion bombardment were also expected to form higher density films. When substrate inclination is applied, the intrinsic compressive stress in the film is increased significantly. This increase effectively enhances the hardness of the sputtering deposited films.

It should be noted that coatings deposited at lower nitrogen content exhibit low hardness. When the P_N increased to 0.7 Pa, the rise in hardness of the (Zr–Ti–Cr–Nb)N coating is explained by the formations of larger amounts of strong Me\N bonds present in the films. Also, high hardness may be due to high content of Cr_2N phase, because the hardness of the Cr_2N coating is higher than that of the CrN coating.

5. CONCLUSIONS

From the preparation of (Zr–Ti–Nb)N, (Zr–Ti–Cr–Nb)N, and (Zr–Ti–Cr–Nb–Si)N coatings by vacuum arc deposition under different pressures of nitrogen and potential bias, it was found that:

1. The (Zr–Ti–Nb)N and (Zr–Ti–Cr–Nb–Si)N nitride coatings include only one phase of solid solution with fcc lattice of NaCl structural type with preferred orientation (111). The structure of the (Zr–Ti–Cr–Nb)N multicomponent coatings is mainly composed of a TiN fcc phase and Cr_2N trigonal modification, which is obviously related to the presence of high concentrations of the elements with low enthalpy of formation of nitrides.
2. The (Zr–Ti–Nb)N, (Zr–Ti–Cr–Nb)N, and (Zr–Ti–Cr–Nb–Si)N coatings have harnesses in the range of 44.5 GPa, 31–39 GPa, and 21–27 GPa, respectively. The mechanical characteristics were improved by applying the higher parameters of deposition (substrate inclination and pressure of nitrogen).

3. The local abrasion of the (Zr–Ti–Cr–Nb–Si)N coatings down to the substrate material occurs when the load reaches a highest value of 46 N, 62 N for (Zr–Ti–Cr–Nb)N coatings, and 66 N for (Zr–Ti–Nb)N.

REFERENCES

Bagdasaryan, A.A., Smirnova, E., Konarski, P., Misnik, M., and Zawada, A., The Analysis of Elemental Composition and Depth Profiles of Nitride Nanostructured Coating Based on the TiHfVNbZr High-Entropy Alloy, *J. Nano-Electron. Phys.*, vol. **6**, no. 2, pp. 02028–1, 2014.

Boxman, R.L., Zhitomirsky, V.N., Grimberg, I., Rapoport, L., Goldsmith, S., and Weiss, B.Z., Structure and Hardness of Vacuum Arc Deposited Multi-Component Nitride Coatings of Ti, Zr, and Nb, *Surf. Coat. Technol.*, vol. **125**, pp. 257–262, 2000. DOI: 10.1016/S0257-8972(99)00570-8

Giannozzi, P., Baroni, S., Bonini, N., Calandra, M., Car, R., Cavazzoni, C., Ceresoli, D., Chiarotti, G.L., Cococcioni, M., Dabo, I., Dal Corso, A., de Gironcoli, S., Fabris, S., Fratesi, G., Gebauer, R., Gerstmann, U., Gougoussis, C., Kokalj, A., Lazzeri, M., Martin-Samos, L., Marzari, N., Mauri, F., Mazzarello, R., Paolini, S., Pasquarello, A., Paulatto, L., Sbraccia, C., Scandolo, S., Sclauzero, G., Seitsonen, A.P., Smogunov, A., Umari, P., and Wentzcovitch, R.M., Quantum Espresso: A Modular and Open-Source Software Project for Quantum Simulations of Materials, *J. Phys.: Cond. Mat.*, vol. **21**, pp. 395502–19, 2009. DOI: 10.1088/0953-8984/21/39/395502

Han, J.G., Myung, H.S., Lee, H.M., and Shaginyan, L.R., Evaluation of the High Temperature Characteristics of the CrZrN Coatings, *Surf. Coat. Technol.*, vol. **174-175**, pp. 738–743, 2003. DOI: 10.1016/S0257-8972(03)00565-6

Hasegawa, H., Kimura, A., and Suzuki, T., Microhardness and Structural Analysis of (Ti, Al)N, (Ti, Cr)N, (Ti, Zr)N, and (Ti, V)N Films, *J. Vac. Sci. Technol. A*, vol. 1**8**, no. 3, pp. 1038–1040, 2000. DOI: 10.1116/1.582296

Holleck, H., Material Selection for Hard Coatings, *J. Vac. Sci. Technol. A*, vol. **4**, pp. 2661–2669, 1986. DOI: 10.1116/1.573700

Kim, S.M., Kim, B.S., Kim, G.S., Lee, S.Y., and Lee, B.Y., Structure and Mechanical Properties of Cr–Zr–N Films Synthesized by Closed Field Unbalanced Magnetron Sputtering with Vertical Magnetron Sources, *Surf. Coat. Technol.*, vol. **202**, nos. 22–23, pp. 5521–5525, 2008. DOI: 10.1016/j.surfcoat.2008.06.101

Pal Dey, S. and Deevi, S.C., Single Layer and Multilayer Wear Resistant Coatings of (Ti, Al)N: A Review, *Mater. Sci. Eng. A*, vol. **342**, pp. 58–79, 2003. DOI: 10.1016/S0921-5093(02)00259-9

Pogrebnjak, A.D., Bagdasaryan, A.A., Yakushchenko, I.V., and Beresnev, V.M., The Structure and Properties of High-Entropy Alloys and Nitride Coatings Based on Them, *Russ. Chem. Rev.*, vol. **83**, no. 11, pp. 1027–1061, 2014a. DOI: 10.1070/RCR4407

Pogrebnjak, A.D., Danilionok, M.M., Uglov, V.V., Erdybaeva, N.K., Kirik, G.V., Dub, S.N., Rusakov, V.S., Shypylenko, A.P., Zukovski, P.V., and Tuleushev, Y.Zh., Nanocomposite Protective Coatings Based on Ti–N–Cr/Ni–Cr–B–Si–Fe, Their Structure and Properties, *Vacuum*, vol. **83**, pp. 8235–8239, 2009b. DOI: 10.1016/j.vacuum.2009.01.071

Pogrebnjak, A.D., Shpak, A.P., Beresnev, V.M., Kolesnikov, D.A., Kunitskii, Yu.A., Sobol, O.V., Uglov, V.V., Komarov, F.F., Shypylenko, A.P., Makhmudov, N.A., Demyanenko, A.A., Baidak, V.S., and Grudnitskii, V.V., Effect of Thermal Annealing in Vacuum and in Air on Nanograin Sizes in Hard and Superhard Coatings Zr–Ti–Si–N, *J. Nanosci. Nanotech.*, vol. **12**, no. 12, pp. 9213–9219, 2012. DOI: 10.1166/jnn.2012.6777

Pogrebnjak, A.D., Yakushchenko, I.V., Bagdasaryan, A.A., Bondar, O.V., Krause-Rehberg, R., Abadias, G., Chartier, P., Oyoshi, K., Takeda, Y., Beresnev, V.M., and Sobol, O.V., Microstructure, Physical and Chemical Properties of Nanostructured (Ti–Hf–Zr–V–Nb)N Coatings under Different Deposition Conditions, *Mater. Chem. Phys.*, vol. **147**, no. 3, pp. 1079–1091, 2014b. DOI: 10.1016/j.matchemphys.2014.06.062

Pogrebnyak, A.D., Shpak, A.P., Azarenkov, N.A., and Beresnev, V.M., Structures and Properties of Hard and Superhard Nanocomposite Coatings, *Phys.-Usp.*, vol. **52**, no. 1, pp. 29–54, 2009a [in Russian]. DOI: 10.3367/UFNe.0179.200901b.0035

Poplavsky, V., Luhin, V., and Koltunowicz, T., Composition of Surface Layers Prepared by Ion Beam Assisted Deposition of Catalytic Metals from Pulsed Arc-Discharge Plasma onto Carbon Paper Substrates, *Acta Phys. Pol. A*, vol. **132**, no. 2, pp. 295–298, 2017.

Sobol, O.V., Pogrebnyak, A.D., and Beresnev, V.M., Effect of the Preparation Conditions on the Phase Composition, Structure, and Mechanical Characteristics of Vacuum-Arc Zr–Ti–Si–N Coatings, *Phys. Met. Metall*., vol. **112**, no. 2, pp. 188–195, 2011. DOI: 10.1134/S0031918X11020268

Sundgren, J.E. and Hentzell, H.G.T., A Review of the Present State of Art in Hard Coatings Grown from the Vapor Phase, *J. Vac. Sci. Technol. A*, vol. **4**, no. 5, pp. 2259–2273, 1986. DOI: 10.1116/1.574062

Svito, I.A., Fedotov, A.K., Saad, A., Zukowski, P., and Koltunowicz, T.N., Influence of Oxide Matrix on Electron Transport in $(FeCoZr)_x(Al_2O_3)_{1-x}$ Nanocomposite Films, *J. Alloys Compd*., vol. **699**, no. 30, pp. 818–823, 2017.

Vanderbilt D., Soft Self-Consistent Pseudopotentials in a Generalized Eigenvalue Formalism, *Phys. Rev. B*, vol. **41**, no. 11, pp. 7892–7895, 1990. DOI: 10.1103/PhysRevB.41.7892

Wagner, C.D., *Handbook of XPS*, Minnesota: Physical Electronics Inc., 1995.

Zhang, S., Wang, N., Li, D.J., Dong, L., Gu, H.Q., Wan, R.X., and Sun, X., The Synthesis of Zr–Nb–N Nanocomposite Coating Prepared by Multi-Target Magnetron Co-Sputtering, *Nucl. Instr. Meth. Phys. B*, vol. **307**, pp. 119–122, 2013. DOI: 10.1016/j.nimb.2012.12.067

MICROSTRUCTURE AND TRIBOLOGICAL PROPERTIES OF NITRIDE COATINGS BASED ON Zr, Ti, Cr, Nb, AND Si ELEMENTS [Текст] / A.D. Pogrebnjak, A.A. Bagdasaryan, V.M. Beresnev [та ін.] // High Temp erature Material Processes. — 2017. — №21(3). — С. 261-275.